Master’s Thesis of Damin Lee

Kinetic Modeling for Catalytic Conversion of DME to Gasoline-range Hydrocarbons over ZSM-5

- Mechanistic kinetic modeling and parameter optimization -

제올라이트 촉매 상 DME 로부터 가솔린 영역의 탄화수소 합성 반응의 키네틱 모델링 연구

February 2023

Graduate School of Chemical and Biological engineering
Seoul National University

Damin Lee

Kinetic Modeling for Catalytic Conversion of DME to Gasoline-range Hydrocarbons over ZSM-5

제올라이트 촉매 상 DME 로부터 가솔린 영역의 탄화수소 합성 반응의 키네틱 모델링 연구

지도 교수 이원보

이 논문을 공학석사 학위논문으로 제출함
2023 년 1 월

서울대학교 대학원
화학생물공학부
이 다 민

이다민의 공학석사 학위논문을 인준함
2023 년 1 월

위 원 장 _____ 이 규 태 _____ (인)
부위원장 _____ 이 원 보 _____ (인)
위 원 _____ 남 재 욱 _____ (인)

Abstract

A new kinetic model for the synthesis of gasoline-range hydrocarbons from dimethyl ether over a nanostructured ZSM-5 catalyst was developed based on the dual-cycle reaction mechanism. The production of individual olefin species was described by two independent cycles (olefinic and aromatic), and the model included surface methoxy as an intermediate in the heterogeneous reaction processes. Kinetic parameters for the model were estimated by fitting the experimental data under various conditions in the temperature range of 513–533 K, a space velocity of 2200–10000 L/(kgcat·h), and a pressure of 1–5 bar, using the genetic algorithm. The developed model described the experimental results with a relative error below 15 %, and the estimated kinetic parameters explained the governing behaviors of the reaction. The activation energies of olefinic methylation decreased with increasing chain length, and ethylene was more selectively produced by aromatic cracking, while the olefinic cycle was the main contributor for the production of propylene, in comparison with the aromatic cycle. With the developed model, the dependence of product selectivity on the operating conditions (temperature and pressure) and the evolution of product yields for each species in the reactor could be predicted accurately and precisely.

Keyword : Dimethyl ether; Gasoline-range hydrocarbon; Nanostructured ZSM-5; Detailed kinetic model; Dual-cycle mechanism; Parameter estimation

Student Number : 2021-20073

Contents

Chapter 1. Introduction

The conversion of dimethyl ether (DME) to hydrocarbons has received significant attention in terms of producing possible fuel chemicals from low-carbon reactants, along with the conversion of methanol [1, 2]. Because this is a process that can produce alternative fuels for existing petrochemical-based fuels, it is important in situations where environmental and energy production transformation are a goal around the globe.

Since the discovery of the catalytic conversion of methanol to hydrocarbons in the 1970s, mechanistic and kinetic studies on methanol-to-olefin (MTO) and methanol-to-hydrocarbon (MTH) reactions have been actively conducted. DME, discovered in the reaction medium as an intermediate, began to attract attention as an independent reactant in the 1990s because it can be easily valorized at a relatively low H_2/CO ratio and can be obtained from low-cost feedstocks such as biomass, pet-coke, and coal [3]. Recently, the advantages of DME as a reactant have been highlighted because of its higher reactivity for methylation compared to methanol and lower formation of formaldehyde (known as a precursor for coke formation and catalyst deactivation) in contrast with the reaction of methanol [4-7].

Many studies on the mechanisms associated with the formation of the C-C bonds and the conversion of DME over zeolite catalysts have been conducted [5, 6, 8]. The reaction mainly consists of a direct mechanism during the induction period and a dual-cycle mechanism during the autocatalytic period. Direct C-C bond formation, although the exact path is still in debate, describes that the first olefin product, such as ethylene or propylene, is produced via intermediates from DME reactants on the catalyst surface. Several mechanisms including oxonium ylide, methoxymethyl cation, methoxymethyl methyl, or carbonic acid mechanism, have been suggested, each of which includes specific intermediates; for example, trimethyl oxonium, methoxymethyl, formaldehyde,

or methylacetate[9-12] have been introduced from the surface methoxy group. The microkinetic modeling approach based on the direct mechanism for DTH has been widely used by many researchers because it is an efficient tool for identifying crucial intermediates; Froment and co-workers studied methanol conversion based on oxonium ylide mechanism, and van Veen and co-workers recently presented methoxymethyl mechanism on DME conversion[13-17].

After C-C bonds were formed directly, the autocatalytic nature of the reaction is described by dual-cycle mechanisms, where fast reactions between the reactants and products, called hydrocarbon pools in the reaction medium, constitute two independent autocatalytic cycles (olefinic and aromatic); Methylation and cracking of olefins, methylation and side-chain dealkylation of aromatics, and cyclization, are included in the dual cycle. In each cycle, the species grow in length, and light olefins such as ethylene and propylene are produced independently. The difference in product yield produced by each cycle has been experimentally studied by Svelle et al.[18] and Sun et al.[19]. Macromolecules such as heavy olefins and aromatics which exist in the reaction medium play the role of composite co-catalysts. In the first kinetic studies of the MTH reaction, the autocatalytic step of the reaction was emphasized, and many lumped kinetic models, in which methanol and DME mixtures (oxygenates) repeatedly react with light olefin products, have been presented [20-22]. Currently, the dual-cycle mechanism is universally accepted in these processes involving DTH and MTH [5, 23, 24]. Because the conversion of DME is a complex reaction system in which a wide range of product mixtures are generated, its phenomenological kinetic modeling has been mainly based on the lumping of the product distribution. Dughaither [25] suggested a Langmuir-Hinshelwood-type model to explain that the chain growth of both olefins and aromatic compounds over the HZSM-5 catalyst is based on methylation. Paula Perez-Uriarte et al. [4] presented a kinetic model of the DME-to-olefins (DTO) reaction, where eleven lumps, each with different reaction

rate constants, were considered to reflect the difference in reactivity between methanol and DME, and the effect of the different reactivities of the two reactants on the distribution of products was evaluated using the model.

A kinetic model can be applied to an actual process to design a reactor and build a separation train; Because the detailed kinetic model can provide more accurate information on the composition of individual components, the reliable design of the process becomes feasible. However, in most of the reported models, aromatics (BTX and bulkier polymethyl benzenes) were treated as high hydrocarbons or final products that did not participate in the reaction, or they were oversimplified despite the fact that further reactions were considered; this eliminated the role of the aromatics in the 'cycle' mechanism. In other words, the methylation and dealkylation of aromatics for the production of ethylene and propylene has rarely been studied. Furthermore, additional olefin generation from BTX compounds was not considered in these models.

Ortega et al. [3] presented a kinetic model of DTH consisting of seven lumps under the assumption of a constant concentration of polymethylbenzene during the reaction at steady state when modeling the aromatic cycle. They considered the direct generation of aromatic lumps from oxygenates and the generation of light olefins by direct splitting of the aromatics, not by the aromatic cycle. However, it is known that aromatic compounds are not produced directly from oxygenates but through the hydrogen transfer of higher alkenes, and dealkylation occurs in the side chain of aromatics without complete decomposition.

Although detailed mechanisms for the DTG reaction have been reported in the literature, most of them are limited to the explanation of the experimentally observed behaviors, and lumping of the individual chains has been mostly applied for kinetic rate equations. This study presents a new kinetic model for the DTG reaction on nanostructured ZSM-5, which is not based on the lumping of the products but considers

all individual olefinic product species. To reflect the heterogeneous catalyst reaction, site balance was established for the acidic sites of the catalyst, and a surface methoxy was introduced as a surface intermediate for the production of olefins and chain growth of aromatics. Because the developed model proposes the kinetics of both olefinic and aromatic reactions based on the dual-cycle mechanism, it suggests a better explanation for the concentration of aromatic products and their kinetics.

Chapter 2. Methods

2.1. Characterization methods

The DTH reaction on nanostructured ZSM-5 was carried out in a fixed-bed tubular reactor with an outer diameter of 9.53 mm to develop kinetic equations and estimate kinetic parameters. Before the DTH reaction, 0.4 g of the catalyst was loaded and pre-treated at 773 K for 1 h under N_2 flow at different experimental conditions such as temperatures (513 – 573 K), pressures (1–5 bar), and GHSVs (2200–10000 L/(kg_{cat}·h)) at a fixed molar ratio of DME/N_2 = 5/95 as described in Table S1 in Supplementary Information. The reactor effluents were analyzed by using online gas chromatography (YL 6500 GC, YoungLin) equipped with a DB-Petro capillary column and a Carboxen 1000 packed column connected with a flame ionization detector (FID) and thermal conductivity detector (TCD), respectively. DME conversions and hydrocarbon distributions were calculated based on total carbon balance.

Chapter 3. Results and Discussion

3.1. Operation conditions and results of reaction

As shown in Figure S2, very high SVs and low temperatures below 533 K were responsible for the decreased DME conversion and increased selectivity of C1–C4 light hydrocarbons due to the possible thermal cracking reaction of heavily methylated hydrocarbons. In addition, the undefined hydrocarbons such as polymethylated cyclic components and oxygenates[6, 35, 36] were slightly increased with increases in reaction pressures (from 7.1% at 1 bar to 13.0% at 5 bar when the temperature was 533 K), which can be attributed to the large number of Brønsted acid sites on the nano-structured ZSM-5 surfaces by enhancing the formation rate of high molecular weight hydrocarbons[35]. Therefore, the main hydrocarbons listed in Table S3 were considered for the further derivations of the kinetic equations and parameters.

DME conversion was calculated based on the inlet and effluent of the reactor, while the selectivity of each product was calculated using the carbon numbers, $S_i = \frac{n_{c,i} y_i}{\sum_k n_{c,k} y_k}$ ($n_{c,i}$: number of carbons in species i, y_i : molar fraction of species i in the products) .

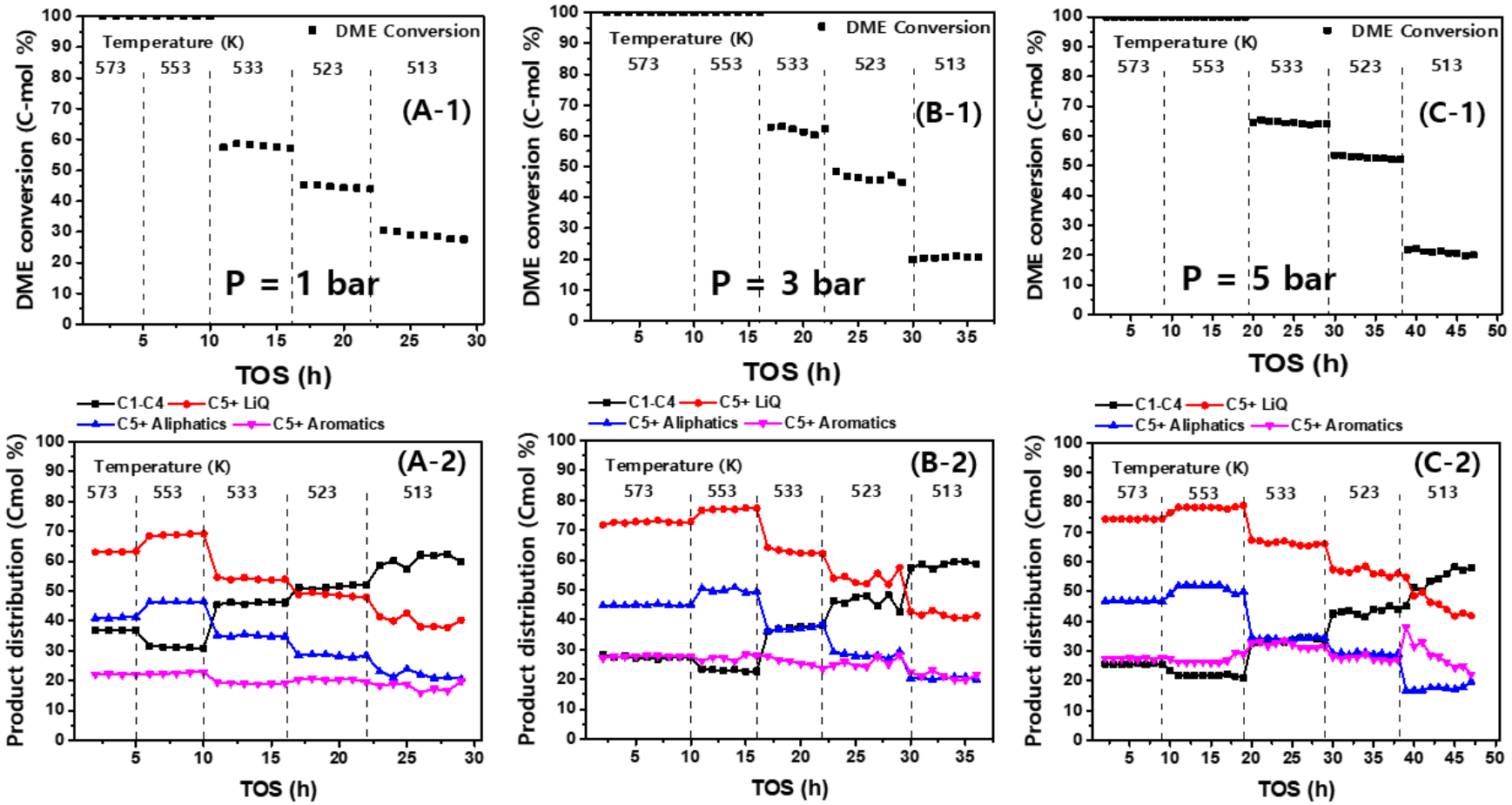

Figure 1. Representative reaction results of (1) DME conversion and (2) product distributions of gaseous and liquid products at different temperatures and pressures such as (A) 1 bar, (B) 3 bar, and (C) 5 bar.

Table 1. Detailed products distributions and DME conversions at 18 different reaction conditions such as temperatures, space velocities, and pressures

[a]Products distributions were verified by using the gaseous effluent chemicals at the reaction conditions of T = 573–513 K, P = 1–5 bar and GHSV = 4400–10000 L/(kg_{cat}·h) with DME/N_2 = 5/95 (mol%), and the abbreviations of m,p,o-X, EMB and TMB stand for m,p,o-Xylene, ethylmethylbenzene and tetramethylbenzene, respectively.

T [K]	SV [L/kg_{cat}/h]	P [bar]	DME Conv. (mol%)	Mole fractions of effluent gases (%)[a]																		
				C1	C2	C3	C4	C5	MTBE	C6	Benzene	C7	Toluene	C8	Ethyl benzene	m,p-X	o-X	C9	EMB	TMB	etc	Carbon balance(%)
573	4400	1	100.0	0.1	3.3	18.7	14.7	12.3	2.9	12.9	0.9	8.5	1.0	4.4	0.2	2.7	1.0	3.0	6.6	1.1	5.7	102.4
553	4400	1	100.0	0.1	4.5	14.7	11.9	11.1	2.8	14.3	0.6	11.0	0.5	7.3	0.1	2.5	1.2	2.7	6.9	0.9	7.1	100.6
533	4400	1	57.8	0.1	5.4	29.9	10.5	6.1	1.3	10.3	0.5	9.6	0.3	6.8	0.0	2.1	0.9	2.2	6.5	1.1	6.2	102.2
523	4400	1	44.6	0.3	7.1	31.4	10.0	5.9	0.7	9.1	0.2	9.2	1.6	3.7	0.0	1.7	1.2	0.8	7.2	1.0	9.0	101.1
513	4400	1	28.8	0.3	5.8	36.1	11.8	5.0	0.8	8.0	0.3	8.5	1.7	3.3	0.1	1.6	1.1	0.8	6.4	0.9	7.4	98.2
573	4400	3	100.0	0.2	1.9	17.1	8.3	14.4	1.2	14.3	1.0	8.7	1.1	4.3	0.2	3.0	1.1	3.1	7.8	1.1	11.3	97.8
553	4400	3	100.0	0.3	3.7	12.1	6.9	12.6	1.3	15.8	0.6	11.9	0.5	6.8	0.1	2.3	1.2	2.7	7.5	0.9	12.8	102.2
533	4400	3	62.0	0.4	8.5	22.2	6.1	7.5	0.5	10.9	0.3	9.9	0.3	6.7	0.0	2.1	1.0	2.2	8.5	1.0	12.0	104.1
523	4400	3	46.0	0.6	9.2	27.0	7.9	6.7	0.2	8.8	0.2	8.3	1.5	3.5	0.0	1.7	1.2	1.0	8.2	1.3	12.8	100.9
513	4400	3	20.0	0.6	6.3	38.8	11.3	3.7	0.4	4.7	0.5	5.4	0.2	4.3	0.0	1.6	0.7	2.1	6.9	1.0	11.1	102.4
573	4400	5	100.0	0.2	1.2	16.9	7.4	14.8	0.8	14.9	0.9	9.4	1.5	4.3	0.3	3.2	1.2	3.5	7.1	1.4	11.0	97.7
553	4400	5	100.0	0.3	3.0	12.2	6.2	13.5	1.0	16.2	0.6	12.1	0.6	6.9	0.1	2.3	1.0	2.8	7.4	0.9	13.0	100.7
533	4400	5	64.5	0.4	8.1	19.2	6.0	7.2	0.4	9.7	0.4	8.8	0.3	6.0	0.0	2.0	1.0	2.4	8.7	1.2	18.1	105.1
523	4400	5	52.9	0.6	9.6	25.7	7.5	7.2	0.3	9.0	0.2	8.4	1.5	3.5	0.0	1.7	1.1	1.0	8.2	1.3	13.2	103.1
513	4400	5	20.9	0.7	6.4	35.8	10.9	3.7	0.5	4.2	0.4	4.5	0.2	3.5	0.0	1.5	0.6	1.7	7.1	1.1	17.2	99.2
533	2200	1	92.9	0.2	5.6	14.1	8.4	9.4	1.5	14.4	0.5	12.0	0.4	7.5	2.3	0.3	1.1	2.6	7.4	1.1	11.2	98.5
533	8800	1	38.6	0.2	4.1	36.1	14.3	5.3	1.6	8.4	0.6	8.1	0.2	5.3	1.4	0.3	0.5	2.4	4.4	1.2	5.6	101.2
533	10000	1	33.5	0.2	4.1	41.4	14.0	4.1	1.5	7.6	0.6	7.5	0.2	5.4	0.0	2.0	0.4	1.6	4.8	0.8	4.0	98.8

3.2. Kinetic mechanism and reaction rates

The reaction path considered in the present study consisted of eight main stages: (1) Surface methoxy formation; (2) DME – methanol equilibrium reaction; (3) ethylene formation; (4) propylene formation; (5) methylation; (6) oligomerization; (7) aromatic cycle; and (8) olefinic cracking. The reaction scheme is as follows:

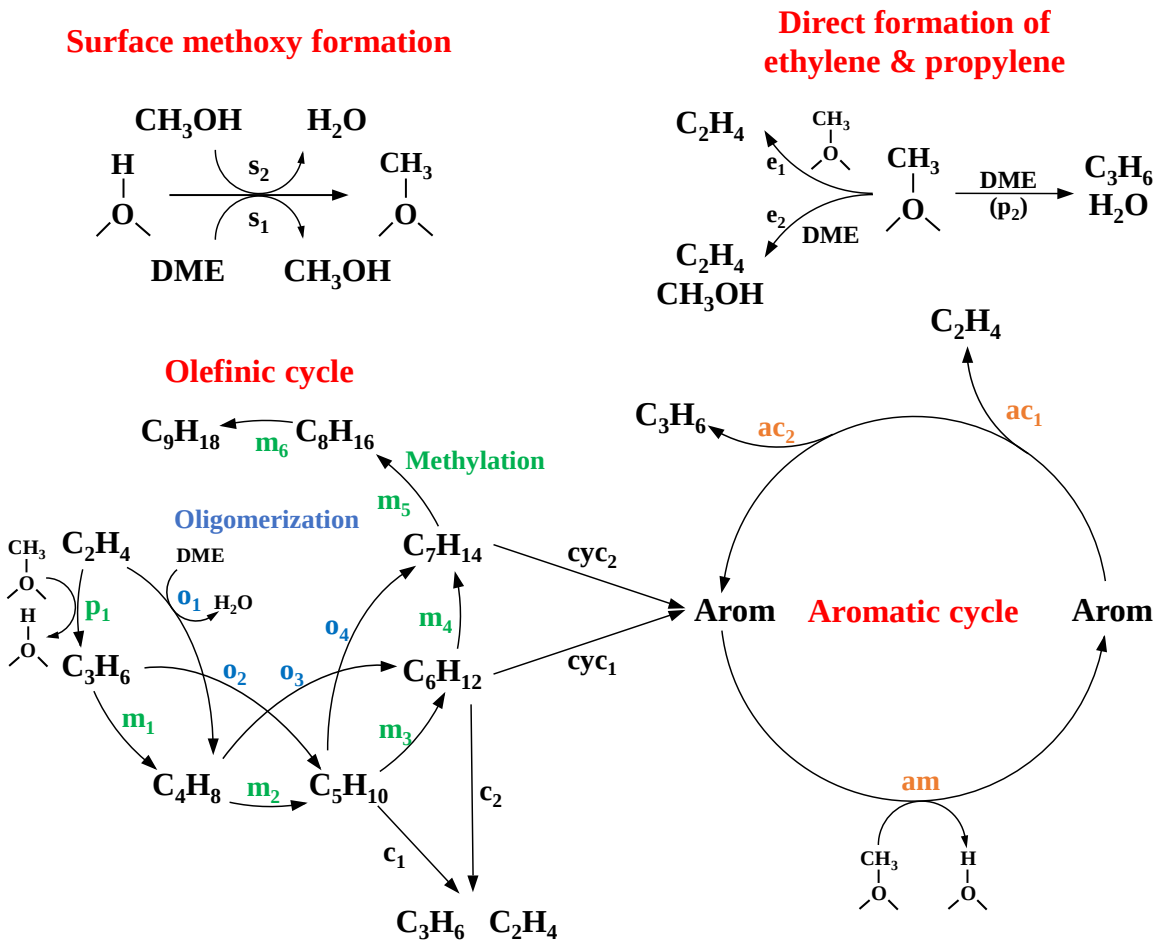

Figure 2. Reaction pathway for DTG over HZSM-5 catalyst considered in the present study. Each label over an arrow denotes the reaction step and the same symbol was used in the subscript of the corresponding reaction in Table 1.

The adsorbate species present on the catalyst surface were DME, methanol, water, ethylene, propylene, and surface methoxy species. The adsorption of DME and methanol onto the catalytic surface leads to the formation of surface methoxy group and further C-C bonds, and water is competitively adsorbed onto the active site, as suggested in several kinetic models in the literature [25, 37, 38]. Notably, surface methoxy groups are important reaction intermediates in the methylation process, and ethylene and propylene are the major product species in the reaction system. The Langmuir-Hinshelwood mechanism was applied to the six species that were adsorbed onto the catalytic surface, while the others in the gas phase were assumed to react with the adsorbate on the catalytic surface; thus, the Eley-Rideal mechanism was considered for these species.

The production of paraffins was neglected based on previous studies showing that the proportion of generated paraffins was insignificant [4]; owing to this, the aliphatic products observed in the present study were assumed to be olefins. In addition, the C1 products observed were assumed to represent MeOH, while byproducts such as CH_4 and CO that might be generated by cracking of DME were excluded from the present study because the amount of C1 products in the experimental data was so small that each species could not be quantified separately.

The detailed elementary steps, based on the reaction pathway shown in Figure 2, and the corresponding reaction rates are provided in Table 2.

Table 2. Elementary reactions steps and rate equations

No.	Formula	Rate laws
1	$\mathrm{DME} + \mathrm{HZ} \rightleftharpoons \mathrm{CH_3 \cdot Z} + \mathrm{CH_3OH}$	$r_{s1} = k_{s1} p_{DME} \theta_{HZ} - k_{s1}^{rev} p_{\mathrm{CH_3OH}} \theta_{\mathrm{CH_3}})$
2	$\mathrm{CH_3OH} + \mathrm{HZ} \rightleftharpoons \mathrm{CH_3 \cdot Z} + \mathrm{H_2O}$	$r_{s2} = k_{s2} p_{\mathrm{CH_3OH}} \theta_{HZ} - k_{s2}^{rev} p_{\mathrm{H_2O}} \theta_{\mathrm{CH_3}})$
3	$\mathrm{DME} + \mathrm{H_2O} \rightleftharpoons 2\mathrm{CH_3OH}$	$r_{md} = k_{md}(p_{\mathrm{H_2O}} p_{DME} - \frac{1}{K_{md}} p_{\mathrm{CH_3OH}}^2)$
4	$\mathrm{CH_3 \cdot Z} + \mathrm{CH_3 \cdot Z} \xrightarrow{k_{E1}} C_2^{=} + 2HZ$	$r_{e1} = k_{e1} \theta_{\mathrm{CH_3}} \theta_{\mathrm{CH_3}}$
5	$\mathrm{CH_3 \cdot Z} + \mathrm{DME} \xrightarrow{k_{E2}} C_2^{=} + \mathrm{CH_3OH} + HZ$	$r_{e2} = k_{e2} p_{DME} \theta_{\mathrm{CH_3}}$
6	$\mathrm{CH_3 \cdot Z} + C_2^{=} \xrightarrow{k_{P1}} C_3^{=} + HZ$	$r_{p1} = k_{p1} p_{C_2^{=}} \theta_{\mathrm{CH_3}}$
7	$\mathrm{CH_3 \cdot Z} + \mathrm{DME} \xrightarrow{k_{P2}} C_3^{=} + \mathrm{H_2O} + HZ$	$r_{p2} = k_{p2} p_{DME} \theta_{\mathrm{CH_3}}$
8	$\mathrm{CH_3 \cdot Z} + C_3^{=} \xrightarrow{k_{M1}} C_4^{=} + HZ$	$r_{m1} = k_{m1} p_{C_3^{=}} \theta_{\mathrm{CH_3}}$
9	$\mathrm{CH_3 \cdot Z} + C_4^{=} \xrightarrow{k_{M2}} C_5^{=} + HZ$	$r_{m2} = k_{m2} p_{C_4^{=}} \theta_{\mathrm{CH_3}}$
10	$\mathrm{CH_3 \cdot Z} + C_5^{=} \xrightarrow{k_{M3}} C_6^{=} + HZ$	$r_{m3} = k_{m3} p_{C_5^{=}} \theta_{\mathrm{CH_3}}$
11	$\mathrm{CH_3 \cdot Z} + C_6^{=} \xrightarrow{k_{M4}} C_7^{=} + HZ$	$r_{m4} = k_{m4} p_{C_6^{=}} \theta_{\mathrm{CH_3}}$
12	$\mathrm{CH_3 \cdot Z} + C_7^{=} \xrightarrow{k_{M5}} C_8^{=} + HZ$	$r_{m5} = k_{m5} p_{C_7^{=}} \theta_{\mathrm{CH_3}}$
13	$\mathrm{CH_3 \cdot Z} + C_8^{=} \xrightarrow{k_{M6}} C_9^{=} + HZ$	$r_{m6} = k_{m6} p_{C_{8,9}^{=}} \theta_{\mathrm{CH_3}}$
14	$\mathrm{DME \cdot HZ} + C_2^{=} \xrightarrow{k_{O1}} C_4^{=} + \mathrm{H_2O} + HZ$	$r_{o1} = k_{o1} p_{C_2^{=}} \theta_{DME}$
15	$\mathrm{DME \cdot HZ} + C_3^{=} \xrightarrow{k_{O2}} C_5^{=} + \mathrm{H_2O} + HZ$	$r_{o2} = k_{o2} p_{C_3^{=}} \theta_{DME}$
16	$\mathrm{DME \cdot HZ} + C_4^{=} \xrightarrow{k_{O3}} C_6^{=} + \mathrm{H_2O} + HZ$	$r_{o3} = k_{o3} p_{C_4^{=}} \theta_{DME}$
17	$\mathrm{DME \cdot HZ} + C_5^{=} \xrightarrow{k_{O4}} C_7^{=} + \mathrm{H_2O} + HZ$	$r_{o4} = k_{o4} p_{C_5^{=}} \theta_{DME}$
18	$C_6^{=} \xrightarrow{k_{Cyc}} Ar + 3\mathrm{H_2}$	$r_{cyc1} = k_{cyc1} p_{C_6^{=}}$
19	$C_7^{=} \xrightarrow{k_{Cyc2}} Ar + 3\mathrm{H_2}$	$r_{cyc2} = k_{cyc2} p_{C_7^{=}}$
20	$\mathrm{CH_3 \cdot Z} + \mathrm{Ar} \xrightarrow{k_{AM}} Ar + HZ$	$r_{am} = k_{am} p_{Ar} \theta_{\mathrm{CH_3}}$
21	$\mathrm{Ar} \xrightarrow{k_{AC1}} Ar + C_2^{=}$	$r_{ac1} = k_{ac1} p_{Ar}$
22	$\mathrm{Ar} \xrightarrow{k_{AC2}} Ar + C_3^{=}$	$r_{ac2} = k_{ac2} p_{Ar}$
23	$C_5^{=} \xrightarrow{k_{C1}} C_2^{=} + C_3^{=}$	$r_{c1} = k_{ac1} p_{C_5^{=}}$
24	$C_6^{=} \xrightarrow{k_{C2}} 2\, C_3^{=}$	$r_{c2} = k_{c2} p_{C_6^{=}}$

The acid sites (HZ) of the catalyst were active, and adsorption was assumed to follow the Langmuir-Hinshelwood-Hougen-Watson (LHHW) mechanism. The site balance is developed as follows:

$$\theta_{HZ} = 1 - \theta_{\mathrm{CH_3}} - \theta_{\mathrm{CH_3OH}} - \theta_{DME} - \theta_{\mathrm{H_2O}} - \theta_{C_2^{=}} - \theta_{C_3^{=}} \quad (1)$$

$$\theta_{HZ} = \frac{1-\theta_{\mathrm{CH_3}}}{1+X} \qquad \text{where } X = \sum_{i=1}^{5} K_i p_i \tag{2}$$

$$r_{\theta_{\mathrm{CH_3}}} = r_{s1} + r_{s2} - 2r_{e1} - r_{e2} - \sum_{i=1}^{2} r_{pi} - \sum_{i=1}^{6} r_{mi} - 9r_{am} \approx 0 \tag{3}$$

$$\theta_i = \frac{1-\theta_{\mathrm{CH_3}}}{1+X} K_i p_i \ \ (\ \mathrm{i} = \mathrm{CH_3OH, DME, H_2O}, C_2^{=}, C_3^{=}) \tag{4}$$

In the acidic site balance equation (Equation 1), θ_i is the surface coverage occupied by species *i*. The surface methoxy formation was assumed to be at a pseudo-steady-state (PSSA), and the net reaction rate was assumed to be zero, where $\theta_{\mathrm{CH_3}}$ can be calculated by solving the equation (Equation 3), using a relationship between methoxy coverage and the empty site fraction (Equations 3). The surface coverage of the other adsorbate species and empty sites were obtained with respect to the equilibrium constant and partial pressure of each species (Equations 4).

The methylation reaction proposed in the present study follows a stepwise pathway [16, 25, 39] including the generation of a surface methoxy group from methanol and DME, with water and methanol as byproducts. The reversible reaction between DME and methanol should be considered. Several previous studies have assumed that DME and methanol quickly reach equilibrium and participate in subsequent product-generating reactions; however, recent studies [5] have shown that both materials do not reach equilibrium, based on the difference between theoretically calculated and observed water flow rates. Therefore, in this study, the reaction was assumed in the kinetic regime, and the kinetic parameters of both forward and reverse reactions were considered. The forward reaction rate constant was estimated, and the reported equilibrium constant as a function of temperature was used to calculate the reverse rate constant [4]:

$$K_{md}^{eq} = \exp(-9.76 + \frac{3200}{\mathrm{T}} + 1.07\log\mathrm{T} - 6.6 * 10^{-4}T + 4.9 * 10^{-8}T^2 + \frac{6500}{T^2}) \tag{5}$$

Although methanol, generated from DME, participates in the surface methoxy group generation reaction (s_2), many studies have concluded that DME has a significantly high contribution to the generation of products in terms of the reactivity of the oxygenates [4, 6, 40]. Therefore, it was assumed that methanol only participated in generating the methoxy group and was not involved in the rest of the reaction.

The generation of the primary products, ethylene and propylene, comprises of two paths. First, ethylene is produced by the reaction of two methoxy groups generated from DME/methanol (e_1), and ethylene and methanol are produced by the reaction of DME with a surface methoxy group (e_2). Next, propylene is produced by the reaction of ethylene with a surface methoxy group (p_1), and by the reaction of DME with a surface methoxy group (p_2).

Higher olefins are sequentially generated via methylation by the surface methoxy species (m_1–m_6). There is also an oligomerization process via the addition of DME (o_1–o_4), where the chain length of the reactant olefin increases by two, with one molecule of water escaping.

The production of light olefins by cracking of higher olefins in the olefinic cycle was considered, in which ethylene and propylene are produced from pentene (c_1) and hexene (c_2), respectively. Because higher alkenes are not considered adsorbates in the present model, their cracking was assumed to be a gas-phase reaction.

The aromatic cycle includes the formation (cyc_1, cyc_2), methylation (am), and cracking (ac_1, ac_2) of the monocyclic aromatic hydrocarbons. Previously reported models usually do not include aromatic lumps or tend to oversimplify the generation and cracking of aromatics. For example, Ortega et al. [3] presented a kinetic model of DME conversion into hydrocarbons, in which ethylene and propylene are generated from the olefin and aromatic pool cycles, respectively. They assumed that the aromatic lump is directly generated from oxygenates, whereas the generation of light olefins results from the direct

splitting of aromatics, which does not reflect the mechanism by which light olefins are generated by the aromatic cycle.

For simplicity, all polymethylbenzene products, including BTX aromatics, were lumped together as aromatics. First, aromatics are created by cyclization of hexene and heptene, leading to the production of hydrogen as a byproduct. The methylation reaction by a surface methoxy group makes the aromatic bulkier, whereas the side chain of aromatics is dealkylated by cracking reactions to produce ethylene and propylene. Notably, reactions in the aromatic cycle are approached as gas-phase reactions.

It should be noted that other species, such as polymethylated cyclopentadiene and benzene, can undergo methylation reactions, especially in the aromatic cycle[6], and can also undergo cracking and generation of light olefins[36]. However, as shown in Table S3 of the Supplementary Information, the polymethylated products were grouped as the etc product and couldn't be identified separately. Therefore, the exact methylating and cracking reaction pathways for each polymethylated product were excluded in the present study. In addition, if more than two reaction pathways for one product are considered, the degree of freedom for the estimated parameters becomes higher than one, indicating that the independent estimation of the parameters cannot be achieved, especially when considering the limited number of experimental conditions in the present study. This feature means that there is a clear limitation in our model. In addition, it is reported that other oxygenate intermediates, such as formaldehyde, ketene, and acetate, are formed[9, 35]. However, their amount was observed insignificantly in the experimental data, and thus, they were included in the etc product (cf. Table S3) and their contribution to the reaction pathways was not considered in the present study.

According to the dual-cycle mechanism, aromatic species settle in the bulk structure of the zeolite catalyst and act as catalysts that generate light olefins by the repeated growth and dealkylation of their side chains. It is known that as the chain of aromatics becomes

bulkier, it blocks the active sites of the catalyst and becomes coke. However, because deactivation was not observed in the experiments conducted in this study, it was assumed that the rate of carbon unit addition to the aromatic lump by methylation was almost the same as that of the carbon unit leaving the aromatic lump by dealkylation, which results in a pseudo-steady state assumption. Therefore, the closed relation for the partial pressure of the aromatic lump was obtained as follows:

$$\frac{\mathrm{d}(C_{Ar} \cdot F_{Ar})}{\mathrm{dW}} = 6k_{cyc1}p_{C_6^=} + 7k_{cyc2}p_{C_7^=} + 9k_{am}p_{Ar}\theta_{\mathrm{CH_3}} - 2k_{ac1}p_{Ar} - 3k_{ac2}p_{Ar} \approx 0 \quad (6)$$

$$p_{Ar} = \frac{6k_{cyc1}p_{C_6^=} + 7k_{cyc2}p_{C_7^=}}{2k_{ac1} + 3k_{ac2} - 9k_{am}\theta_{\mathrm{CH_3}}} \quad (7)$$

Eleven species (or lumps) were considered: DME, methanol, water, ethylene ($C_2^=$), propylene ($C_3^=$), butene ($C_4^=$), pentene ($C_5^=$), hexene ($C_6^=$), heptene ($C_7^=$), octene ($C_8^=$), nonene ($C_9^=$), and a lump of aromatics. Lumping of higher olefins was avoided by developing a model that thoroughly explains the experimentally observed product distribution. All kinetic parameters for each reaction were estimated using experimental data, except for the formation of aromatics by hexene and heptane (r_{cyc1}, r_{cyc2}), which were assumed to share the same kinetic parameters.

3.3. Parameter estimation

An ideal flow with no radial gradients was assumed for the mass balance in the reactor, and neither the energy balance nor the pressure drop were considered under the assumptions of isothermal and isobaric operations.

$$\frac{\mathrm{d}F_i}{\mathrm{dz}} = \left(\sum_j \nu_{j,i} r_j\right)\rho_b A_r \quad (8)$$

where F_i is the molar flow rate of species i, r_j is the jth reaction rate, $\nu_{j,i}$ is the stoichiometric coefficient for the jth reaction of species i, ρ_b is the bulk density of the catalyst, A_r is the cross-sectional area of the reactor, and z is the z-coordinate of the reactor.

As the pseudo-steady-state assumption was applied to the aromatic lump, the following balance equation was used:

$$\frac{\mathrm{d}F_{Ar}}{\mathrm{dz}} = \frac{F_{total}}{p_{total}}\frac{\mathrm{d}p_{Ar}}{\mathrm{dz}} + \frac{p_{Ar}}{p_{total}}\frac{\mathrm{d}F_{total}}{\mathrm{dz}} \tag{9}$$

The adsorption equilibrium constant of species i over the modified HZSM-5 catalyst was obtained using the van't Hoff equation as follows:

$$K_i = A_i \exp(\frac{-\Delta H_i}{RT}) \tag{10}$$

where A_i, ΔH_i, R, and T are the pre-exponential factor, standard enthalpy of adsorption for species i, gas constant, and temperature, respectively.

The reaction rate constants followed the Arrhenius equation:

$$k_j = k_{j0} \exp(\frac{-E_{aj}}{RT}) \tag{11}$$

where k_{j0} and E_{aj} represent the pre-exponential factor and the activation energy, respectively.

To estimate the kinetic parameters of such a highly nonlinear model, the genetic algorithm (GA) was applied, and the GA solver in MATLAB R2020 (MathWorks, Inc.)

was used, where optimization was used to minimize the following objective function (OF):

$$\mathrm{OF} = \sum_{j=1}^{n_{ex}} \sum_{i=1}^{n_s} \left(\frac{y_{ij,exp} - y_{ij,cal}}{y_{ij,exp}}\right)^2 + \sum_{j=1}^{n_{ex}} \left(\frac{x_{j,exp} - x_{j,cal}}{x_{j,exp}}\right)^2 \tag{12}$$

Here, y_{ij} is a molar fraction of species i in the reactor effluent under the jth experimental condition, and the subscript 'exp' and 'cal' denote the experimental and the calculated values, respectively. x_j represents the DME conversion (%) under the jth experimental condition, and n_s and n_{ex} denote the number of components in the model and number of experiments, respectively. The boundaries of the parameters were set as $A_i > 0$, $\Delta H_i < 0$, and $E_{aj} > 0$.

The initial population for the GA was randomly distributed in the primary approximation, and the results were reused as the initial parameters in the GA with parameter boundaries set at $\pm 50\%$ of the values.

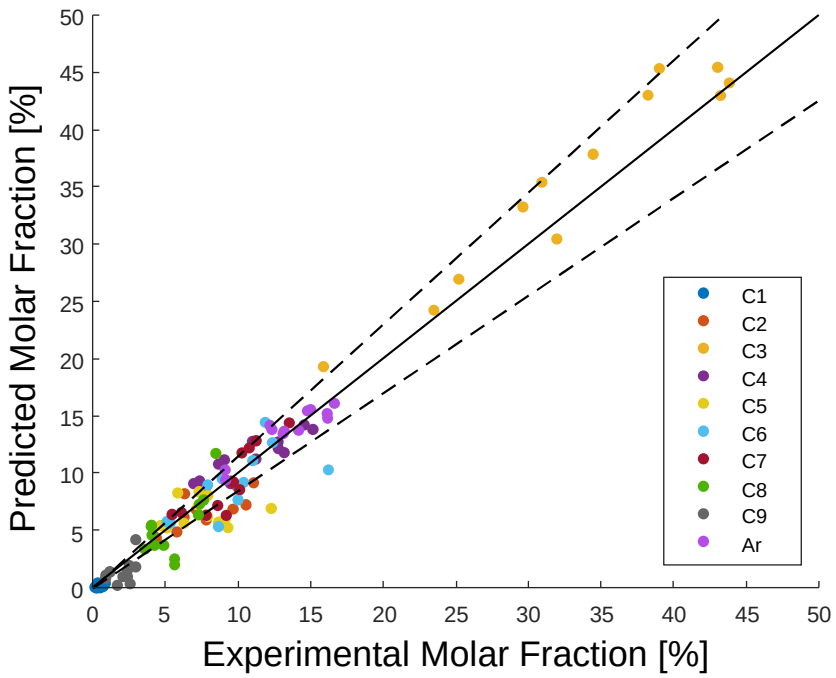

Figure 3. Parity plot of experimental data and simulated results. The dashed line represents a ±15% error margin.

A comparison between the effluent molar fractions from the experimental data and the model calculations is provided in a parity plot (Figure 3). Most of the simulation results were within the ±15% bands, corroborating the satisfactory performance of the proposed model. Most of the deviations were observed for the C1, C8, and C9 species, which had comparatively low molar fractions. This discrepancy may be due to the assumptions used in the model for simplicity. The C1 species in the model considers only methanol, while CH_4 and CO might exist in the DTG reaction owing to the cracking of DME. However, because the amount of C1 species produced under the experimental conditions was less than 0.7 mol%, it was difficult to identify all the C1 species in detail, and thus, only methanol and the corresponding reaction were considered in the model, excluding CH_4 and CO. Perez-Uriarte [4] reported the importance of the cracking step under conditions above 673 K and a short residence time. However, the proposed model considers the formation of C9 species by the methylation of C8 without inclusion of its cracking. Consequently, this model mismatch might result in deviations for the C9 species. Although C8 species are both formed and consumed via methylation, their cracking is excluded in the model, which may lead to a model mismatch.

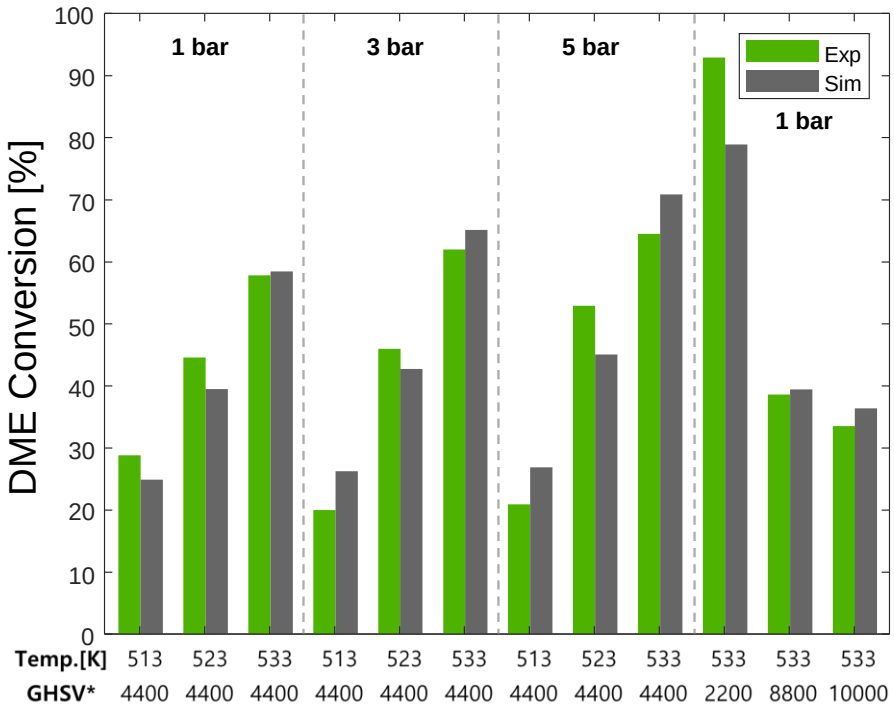

Figure 4. Comparisons of DME conversion between experimental data and simulated results under each operating condition. Entry numbers start from left to right. The units of measurement for GHSV are L/(kg_{cat}·h).

The experimental and simulated DME conversion values for each reaction condition are shown in Fig. 4. Although the mean of the absolute relative errors was 12.38%, there were some differences, possibly due to measurement errors. At low temperatures (513 K), negative effects caused by pressure were observed (entries 1, 4, and 7) and at higher temperatures, positive effects were observed (entries 2, 5, and 8 at 523 K; entries 3, 6, and 9 at 533 K). This inconsistency might indicate measurement errors in the experiment, leading to large deviations.

A large negative error was observed for entry 10 (low SV). In the comparison of the conversions with decreasing SV (increasing residence time), it was observed that the value at an SV of 2,200 L/(kg_{cat}·h) slightly deviated from the trend of the change.

The comparison of the selectivities between experimental data and simulated results

is provided in Figure S3 of the Supplementary Information. To confirm the validity of predictions, selectivity in the experiments was plotted (Figure 7). The tendency of species to change under varying conditions was the same as predictions as described above. Particular deviation was the case of propylene (second bar in yellow) in Figure .a, where the selectivity of the species is somewhat smaller than the equivalent prediction and deviates the tendency to decrease with pressure rise.

Table 3. Estimated kinetic parameters

Adsorption equilibrium constants		A_i [1/bar]	ΔH_i [kJ/mol]
Adsorption	DME	206.9	-20.9
	MeOH	143.5	-1.83
	H_2O	242.0	-1.86
	ethylene	162.4	-76.1
	propylene	227.9	-2.02
Kinetic reaction rate constants		k_{j0}*	E_a[kJ/mol]
Surface methoxy formation	s_1	1.227	121.9
	s_1^{rev}	2.211×10^2	205.6
	s_2	1.692×10^3	154
	s_2^{rev}	10.55	195.4
DME-methanol dehydration	md	8.323×10^{-4}	286.1
Ethylene from direct mechanism	e_1	3.422×10^3	201.0
	e_2	3.496×10^1	199.9
Propylene from direct mechanism	p_1	6.512×10^2	9.059
	p_2	5.646×10^2	200.0
Methylation with surface methoxy	m_1	3.474×10^3	153.2
	m_2	7.568×10^3	122.1
	m_3	9.692×10^3	75.77
	m_4	8.618×10^3	76.83
	m_5	4.263×10^3	95.39

	m_6	1.994×10^{3}	94.53
Oligomerization with DME	o_1	7.487×10^{-1}	310.2
	o_2	1.446×10^{-3}	284.5
	o_3	5.974×10^{-1}	316.5
	o_4	2.146×10^{-5}	243.5
Aromatics cycle	cyc_1	2.572×10^{-2}	18.88
	cyc_2	2.572×10^{-2}	18.88
	am	6.34×10^{0}	143.4
	ac_1	1.326×10^{-1}	82.6
	ac_2	5.29×10^{-3}	250.2
Olefinic cracking	c_1	1.561×10^{-5}	10.14
	c_2	1.378×10^{-5}	11.39

The estimated kinetic parameters are listed in Table 3. The kinetic parameters of the elementary reactions in methylation (m_1–m_6) were estimated to have similar orders of magnitude for pre-exponential factors and activation energies, although Ea tended to decrease as the chain length of the reactant increased. A similar tendency for Ea to decrease with increasing chain length was observed in olefin oligomerization with DME (o_1–o_4), except in the case of butene.

Some of the estimated values of the activation energies for methylation (m_1–m_6, o_1–o_4) in the olefinic cycle (75.77-153.2, 243.5–310.2 kJ/mol, respectively) are larger than those reported in theoretical studies of methylation, which are in the range of 45–109 kJ/mol [40-42]. This feature is attributed to the role of methylation in this model, and the methylation step proposed in this work covers both the direct and stepwise methylation results of methanol or DME [40]. In other words, the proposed kinetics are phenomenological, indicating that the kinetic parameters for methylation used in this model are apparent with all the experimental behaviors included.

To produce methoxy intermediates, the pre-exponential factor for methanol

dehydration (s_2) was estimated to be three orders of magnitude larger than that for the reaction using DME. This large difference is attributable to methylation being the only reaction consuming methanol, whereas DME has other reaction routes.

In olefinic cracking (c_1, c_2), the activation energies of the two reactions were estimated to be almost identical, although the values were lower than those for the other reactions. In the case of aromatic cracking (ac_1, ac_2), the pre-exponential factor for ethylene production (ac_1) was approximately 25 times larger than that for propylene production (ac_2), and the activation energy of ac_1 was lower than that of ac_2, indicating a faster reaction rate for ac_1 compared with ac_2. The difference in reactivity for aromatic cracking has also been reported in the literature. Former experimental studies compared the contributions of the two cycles (olefinic and aromatic) to the production of ethylene and propylene, where ethylene is more selectively produced in the aromatic cycle, while propylene is mostly produced in the olefinic cycle [5, 6, 19, 40, 41].

3.4. Sensitivity analysis

Sensitivity analysis was conducted to evaluate the impact of model parameters on product variables. Sensitivity of the variable j to the parameter i ($S_{i,j}$) was defined as a fractional change of a variable to a fractional change of a parameter, without any change in the other parameters[13, 43, 44]:

$$S_{i,j} = \frac{p_i}{v_j}\left(\frac{\partial v_j}{\partial p_i}\right)_{p_{k\neq i}}$$

where, p_i and v_j are the parameter and the variable, respectively, and 10% perturbation in a parameter and the corresponding change in a variable was calculated for sensitivity. The results of the parameters that showed significant sensitivity are provided in Figure 5.

The sensitivity of pre-exponential factors (k_0) of methylation steps is provided in Figure 5a. It was shown that DME conversion was little influenced by the parameters,

and the selectivity of olefin species, C2–C8 had a negative relationship with the parameters for the consumption of each species. Meanwhile, an increase in parameters of methylation of shorter olefinic chains positively affected the selectivity of longer chains, because more short chains were consumed to produce long olefinic chains. C9 species showed relatively large sensitivity to m5 and m6 reaction parameters, probably because they are the only reaction steps explaining the production of the species. Because aromatics is mainly produced from C6 and C7 species in the model, methylation steps m1–m3 (where C6 is produced) showed positive sensitivity while m4–m6 (where C6 is consumed) had a negative one. The sensitivity of activation energies (*Ea*) of the methylation step in Figure 5b showed the opposite tendency with the corresponding pre-exponential factors.

The effects of reaction steps based on the direct mechanism (s1, s2, md, e1, e2, and p2) on the variables were shown in Figures 5c (pre-exponential factors) and 5d (activation energies). The k_0 of the s1 reaction (surface methoxy formation from DME) had the largest sensitivity over all the variables, nearly two orders higher than those of the other methylation parameters. The increase in s1 reaction rate led to a decrease in propylene selectivity, mainly due to the loss of DME contributed to propylene synthesis. The other hydrocarbon products showed a positive relationship with the parameter, due to increased surface methoxy species and methylating reaction. Although the k_0 of the steps other than s1 resulted in low sensitivity of the variables, they showed a similar tendency as the methylation parameters in Figure 5a. Activation energies (Figure 5d) showed the opposite tendency compared to those of the pre-exponential factors (Figure 5c), but the sensitivity of the s1 step was smaller by approximately ten times, while that of the p2 step increased by ten times.

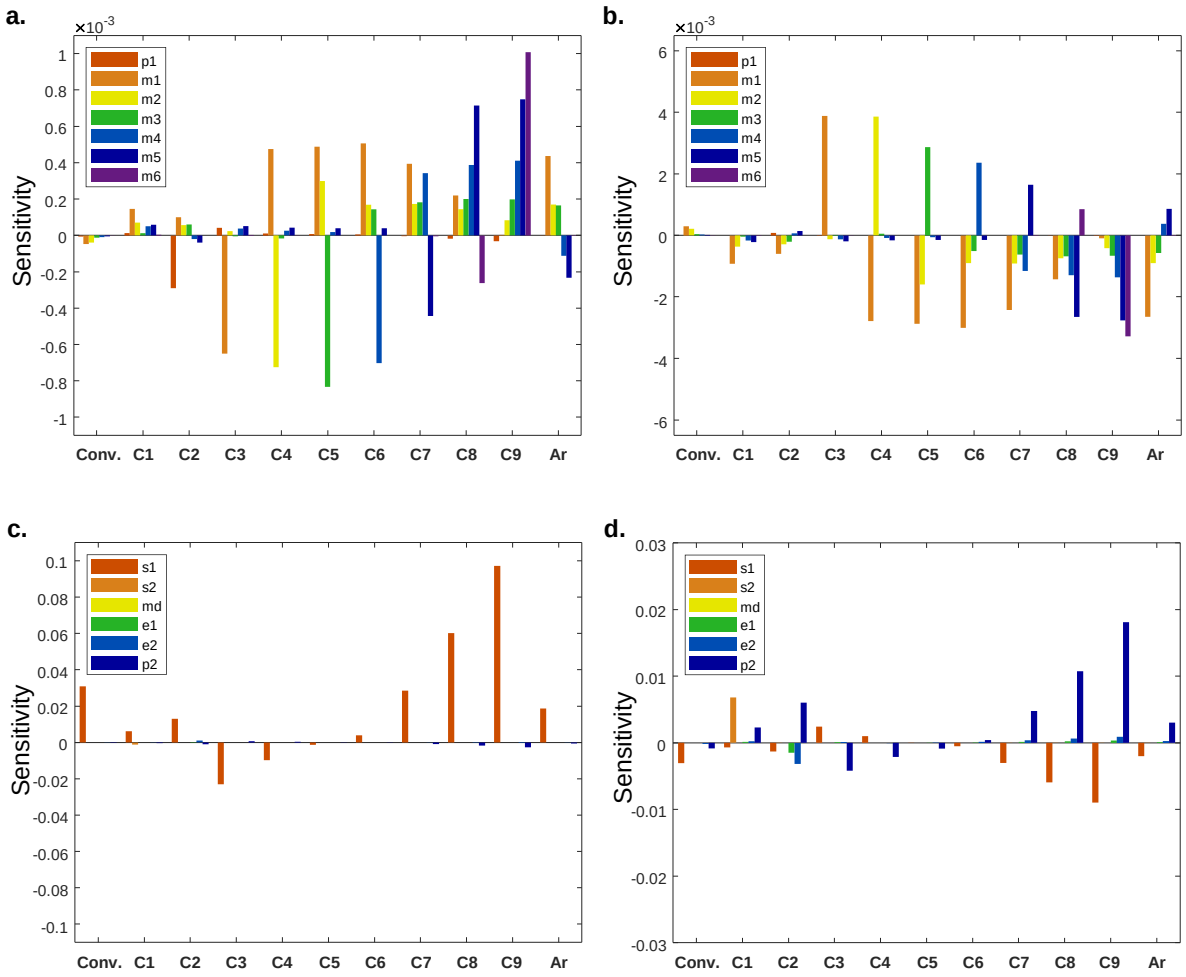

Figure 5. Sensitivity analysis of conversion and selectivities of the products to **(a)** pre-exponential factors and **(b)** activation energies of methylation reactions, and **(c)** pre-exponential factors and **(d)** activation energies of direct mechanisms. Symbols of the reactions can be referred to the Table 1 and Figure 2.

3.5. Effects of operating conditions on product selectivity

Using the kinetic model developed in this study, the effects of temperature and pressure on the conversion and selectivity of each product were evaluated (Figure 5). As the reaction temperature increased, DME conversion increased under all pressures. The selectivities of light olefins under C5 (first, second, and third bars) and aromatic (ninth

bar in purple) compounds decreased with increasing temperature, while the other species showed a positive effect from temperature increase. This feature was also reported in the experimental results for the HZSM-5 catalyst conducted by Paula Perez-Uriarte [4] at temperatures between 598 and 673 K with a pure DME feed.

Conversion increased with pressure at temperatures above 523 K, whereas no significant influence was observed at low temperatures. However, the degree of effect of pressure was smaller than that of temperature. In terms of selectivity, this effect can be described by dividing the selectivities into groups of light olefins (C2–C4), higher olefins above C5 (C5+ aliphatic), and aromatics. For light olefins (C2–C4), the differences between C2, C3, and C4 decreased at high pressures, with a gradual decrease in all species. Meanwhile, in the C5+ aliphatic group, the selectivities were positively influenced by pressure, whereas the higher olefins showed inverse effects from pressure. Finally, the selectivity of aromatics was insignificantly affected by pressure.

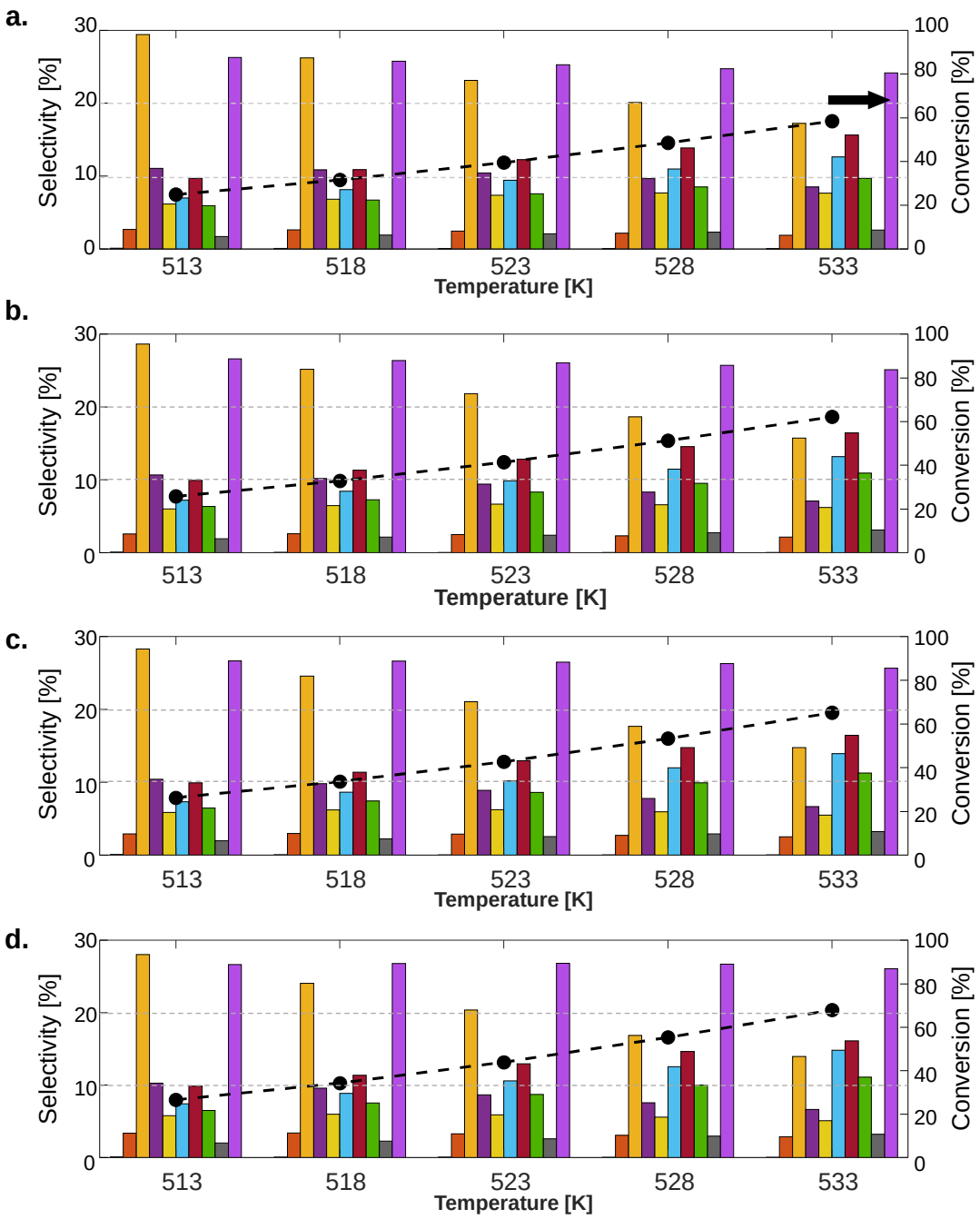

Figure 6. Effects of temperature and pressure on the conversions and the selectivities of each species. Pressures of **(a)** 1, **(b)** 2, **(c)** 3, and **(d)** 4 bar at the SV and feed composition of DME/N_2 were specified to be 4,400 L/(kg_{cat}·h) and 0.05/0.95, respectively. The first eight bars represent C_2 to C_9 (from left to right), and the right-most one denotes the aromatic.

The evolutionary profile of each product in the reactor was simulated using the

developed model. It was shown that the propylene yield sharply increased in the early part of the reactor, while a gradual increase was observed for the other species. As shown in the magnified figure, the yield of ethylene also increased rapidly during the early part of the reactor, whereas olefins above four and aromatic compounds showed a lag at the beginning, and then gradually increased along the reactor axis. This indicates that ethylene and propylene react with the reactants as primary products at the beginning of the reaction.

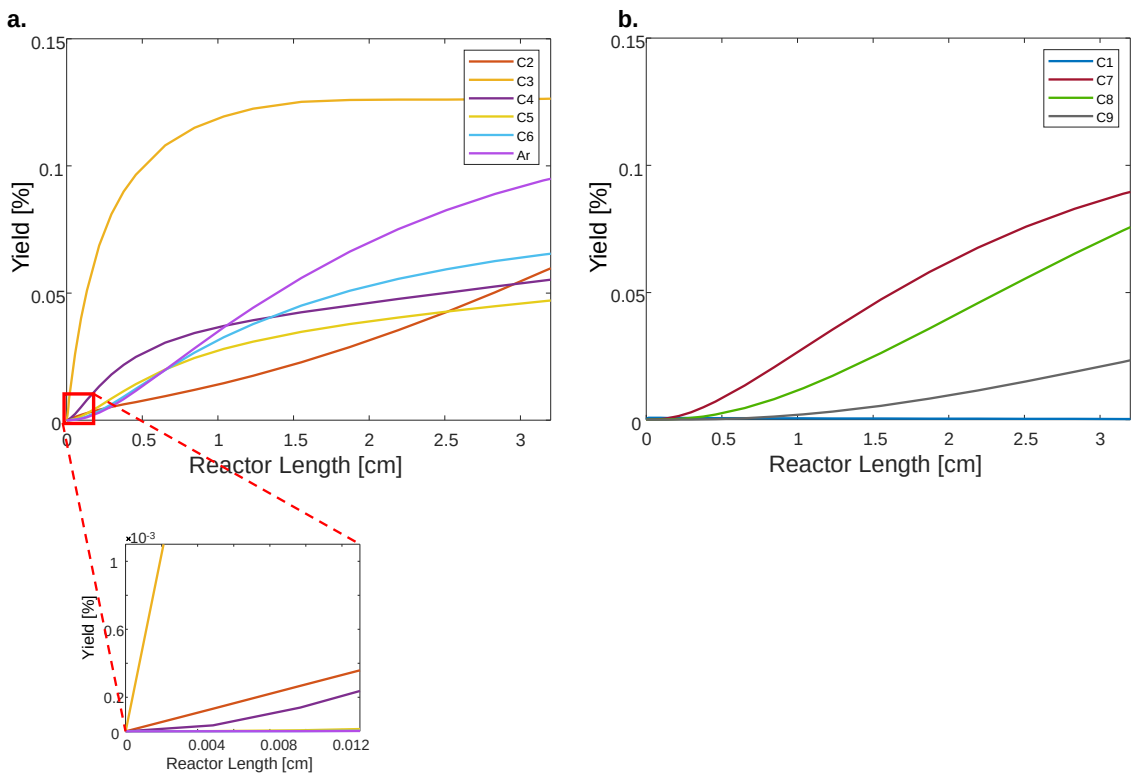

Figure 7. Profiles of the yields of each product in the reactor. Temperature, pressure, SV, and the feed composition of DME/N_2 were specified to be 533 K, 1 bar, 2,200 L/(kg_{cat}·h) and 0.05/0.95, respectively

Chapter 4. Conclusions

A new kinetic model for the DTG process was developed. Based on the dual-cycle mechanism, the reaction pathways comprised of two main cycles: olefinic and aromatic. The reactions between the reactants and surface methoxy intermediates on the catalytic surface were considered to produce longer gaseous products. The model with the estimated kinetic parameters described the experimentally observed behaviors of most of the species in the system (C2–7 olefins and aromatics) within a relative error of 15 %, whereas the large deviations for C1, C8, and C9 species might have resulted from the assumptions made in the model for simplicity. The estimated kinetic parameters for olefinic methylation coincided with the common trend that activation energy decreases with increasing chain length, and the value of the kinetic parameters for aromatic cracking showed that ethylene is more selectively produced in the aromatic cycle, while the olefinic cycle is mostly responsible for the production of propylene. In addition to the analysis of the governing behaviors based on the detailed kinetic mechanisms, the proposed model can be used to evaluate the effects of operating conditions on the product distribution. Thus, the operation strategy to control the growth rate of each product can be determined using this model.

Bibliography

1. C. Ortega and G. Kolb, *Industrial & Engineering Chemistry Research*, 2019, **58**, 22893-22904.
2. S. Lee, M. Gogate and C. J. Kulik, *Fuel Science and Technology International*, 1995, **13**, 1039-1057.
3. C. Ortega, V. Hessel and G. Kolb, *Chemical Engineering Journal*, 2018, **354**, 21-34.
4. P. Pérez-Uriarte, A. Ateka, A. T. Aguayo, A. G. Gayubo and J. Bilbao, *Chemical Engineering Journal*, 2016, **302**, 801-810.
5. J. S. Martinez-Espin, M. Mortén, T. V. W. Janssens, S. Svelle, P. Beato and U. Olsbye, *Catalysis Science & Technology*, 2017, **7**, 2700-2716.
6. I. Yarulina, A. D. Chowdhury, F. Meirer, B. M. Weckhuysen and J. Gascon, *Nature Catalysis*, 2018, **1**, 398-411.
7. F. M. Kirchberger, Y. Liu, P. N. Plessow, M. Tonigold, F. Studt, M. Sanchez-Sanchez and J. A. Lercher, *Proc Natl Acad Sci U S A*, 2022, **119**.
8. S. N. Khadzhiev, M. V. Magomedova and E. G. Peresypkina, *Petroleum Chemistry*, 2014, **54**, 245-269.
9. A. D. Chowdhury, K. Houben, G. T. Whiting, M. Mokhtar, A. M. Asiri, S. A. Al-Thabaiti, S. N. Basahel, M. Baldus and B. M. Weckhuysen, *Angew Chem Int Ed Engl*, 2016, **55**, 15840-15845.
10. J. Li, Z. Wei, Y. Chen, B. Jing, Y. He, M. Dong, H. Jiao, X. Li, Z. Qin, J. Wang and W. Fan, *Journal of Catalysis*, 2014, **317**, 277-283.
11. M. H. WEI WANG, *Accounts of Chemical Research*, 2008, **41**, 895–904.
12. A. B. Wei Wang, Michael Seiler, Michael Hunger, *Journal of the American Chemical Society*, 2003, **125**, 15260–15267.

13. A. H. Motagamwala and J. A. Dumesic, *Chem Rev*, 2021, **121**, 1049-1076.

14. G. F. F. Tae-Yun Park, *Industrial & Engineering Chemistry Research*, 2001, **40**, 4187–4196.

15. T. Omojola and A. C. van Veen, *Chemical Engineering Science*, 2021, **239**.

16. T. Omojola, D. B. Lukyanov and A. C. Veen, *International Journal of Chemical Kinetics*, 2019, **51**, 528-537.

17. S. N. Khadzhiev, M. V. Magomedova and E. G. Peresypkina, *Petroleum Chemistry*, 2015, **55**, 503-521.

18. F. J. Stian Svelle, Jesper Nerlov, Unni Olsbye, Karl-Petter Lillerud, Stein Kolboe, Morten Bjørgen, *Journal of the American Chemical Society*, 2006, **128**, 14770-14771.

19. X. Sun, S. Mueller, Y. Liu, H. Shi, G. L. Haller, M. Sanchez-Sanchez, A. C. van Veen and J. A. Lercher, *Journal of Catalysis*, 2014, **317**, 185-197.

20. A. G. Gayubo, Benito, P.L., Aguayo, A.T., Aguirre, I., Bilbao, J., *The Chemical Engineering Journal and the Biochemical Engineering Journal*, 1996, **63**, 45–51.

21. A. G. Gayubo, Benito, P.L., Aguayo, A.T., Castilla, M., Bilbao, J., *Chemical Engineering Science*, 1996, **51**, 3001–3006.

22. P. H. Schipper, and F.J Krambeck., *Chemical Engineering Science*, 1986, **41.4**, 1013-1019.

23. M. Bjorgen, S. Svelle, F. Joensen, J. Nerlov, S. Kolboe, F. Bonino, L. Palumbo, S. Bordiga and U. Olsbye, *Journal of Catalysis*, 2007, **249**, 195-207.

24. U. Olsbye, M. Bjørgen, S. Svelle, K.-P. Lillerud and S. Kolboe, *Catalysis Today*, 2005, **106**, 108-111.

25. A. S. Dughaither, *Electronic Thesis and Dissertation Repository*, 2014.

26. S. KS, *Jounal of porous materials*, 1995, **2**, 5-8.

27. J. Wei, R. Yao, Q. Ge, D. Xu, C. Fang, J. Zhang, H. Xu and J. Sun, *Applied*

Catalysis B: Environmental, 2021, **283**.

28. Y.-P. Guo, H.-J. Wang, Y.-J. Guo, L.-H. Guo, L.-F. Chu and C.-X. Guo, *Chemical Engineering Journal*, 2011, **166**, 391-400.
29. Y. K. Hwang, J. S. Chang, S. E. Park, D. S. Kim, Y. U. Kwon, S. H. Jhung, J. S. Hwang and M. S. Park, *Angew Chem Int Ed Engl*, 2005, **44**, 556-560.
30. B. G. Martins G, Bisio C, Coluccia S, Pastore H, Marchese L, *Journal of physical chemistry*, 2008, **112**, 7193-7200.
31. W. Dai, L. Yang, C. Wang, X. Wang, G. Wu, N. Guan, U. Obenaus, M. Hunger and L. Li, *ACS Catalysis*, 2018, **8**, 1352-1362.
32. M. Shamzhy, B. Gil, M. Opanasenko, W. J. Roth and J. Čejka, *ACS Catalysis*, 2021, **11**, 2366-2396.
33. K. Góra-Marek, K. Tarach and M. Choi, *The Journal of Physical Chemistry C*, 2014, **118**, 12266-12274.
34. C. Liu, J. Su, S. Liu, H. Zhou, X. Yuan, Y. Ye, Y. Wang, W. Jiao, L. Zhang, Y. Lu, Y. Wang, H. He and Z. Xie, *ACS Catalysis*, 2020, **10**, 15227-15237.
35. A. D. Chowdhury and J. Gascon, *Angew Chem Int Ed Engl*, 2018, **57**, 14982-14985.
36. M. J. Wulfers and F. C. Jentoft, *ACS Catalysis*, 2014, **4**, 3521-3532.
37. M. J. Azarhoosh, R. Halladj and S. Askari, *Journal of Physics: Condensed Matter*, 2017, **29**, 425202.
38. A. G. Gayubo, Andrés T Aguayo, Angel L Morán, Martín Olazar, and Javier Bilbao., *AIChE Journal*, 2002, **48**, 1561-1571.
39. M. R. Gogate, *Petroleum Science and Technology*, 2019, **37**, 28-37.
40. S. Svelle, M. Visur, U. Olsbye, Saepurahman and M. Bjørgen, *Topics in Catalysis*, 2011, **54**, 897-906.
41. S. Svelle, Stein Kolboe, Ole Swang, and Unni Olsbye, *The Journal of Physical*

Chemistry. B 2005, **109.26**, 12874-12878.

42. I. M. Hill, S. A. Hashimi and A. Bhan, *Journal of Catalysis*, 2012, **285**, 115-123.
43. L. A. Alcázar and J. Ancheyta, *Chemical Engineering Journal*, 2007, **128**, 85-93.
44. C. T. Campbell, *ACS Catalysis*, 2017, **7**, 2770-2779.

Abstract in Korean (국문초록)

나노구조의 ZSM-5 촉매 상에서 다이메틸 에터(DME)로부터 가솔린 영역의 탄화 수소를 합성하는 반응에 대한 새로운 키네틱 모델을 이중 사이클 반응 메커니즘에 기반하여 제시하였다. 개별 올레핀 성분들의 생성은 두 종류의 독립적인 사이클(올레핀 기반 및 방향족 기반)으로 설명하였고, 모델에 반응중간물인 표면 메톡시 그룹을 도입하여 불균일계 반응 특성을 반영하고자 하였다. 모델의 키네틱 파라미터는 유전 알고리즘을 통해 513-533 K 의 온도 범위, 2200-10000 L/(kgcat·h)의 공간 속도 범위, 1-5 bar 의 압력 범위를 가진 다양한 운전 조건 하에서 얻어진 실험 데이터에 피팅시켜 얻어냈다. 얻어진 모델은 15% 이하의 상대 오차를 가지고 실험 결과를 설명하였으며 추정된 키네틱 파라미터들을 통해 반응의 지배적인 행동을 설명할 수 있었다. 올레핀 기반의 메틸화 단계에서 활성화 에너지는 반응물의 사슬 길이가 증가함에 따라 감소하였고, 에틸렌은 방향족의 분해에 의해 더 선택적으로 생성이 되는 반면 프로필렌은 올레핀 기반 사이클에서 주로 생성됨을 확인할 수 있었다. 얻어진 모델을 통해 온도, 압력의 운전 조건에 대한 생성물의 선택도 의존성을 확인하였으며 반응기 내에서 각 성분의 분율 변화를 정확하게 예측할 수 있었다.

주요어 : 다이메틸 에터; 가솔린 영역의 탄화수소; 나노 구조 ZSM-5; 키네틱 모델링; 반응 메커니즘; 파라미터 추정

학 번 : 2021-20073